PART I

ASTRONOMICAL BACKGROUND

1 High energy astrophysics – an introduction

1.1 High energy astrophysics and modern physics and astronomy

The revolution in astronomy, astrophysics and cosmology since the end of the Second World War in 1945 has been driven by the opening up of the whole of the electromagnetic spectrum for astronomical observations. This revolution would not have been possible without the development of new techniques and technologies for making astronomical observations from the ground and from space. Hand in hand with these developments have been major advances in laboratory physics and the development of high speed computers. It is the combination of all these factors which has led to dramatic advances in the astrophysical and cosmological sciences.

Among the most important of the new disciplines is *high energy astrophysics*. I take this term to mean the astrophysics of high energy processes and their application in astrophysical and cosmological contexts. These processes, their application in astrophysics and how they lead to some of the most challenging problems of contemporary physics, are the subjects of this book. For example, we need to explain how the massive black holes present in the nuclei of active galaxies can be studied, how charged particles are accelerated to extremely high energies in astronomical environments, the origins of enormous fluxes of high energy particles and magnetic fields in active galaxies, the physical processes in the interiors and environments of neutron stars, the nature of the dark matter, the expected fluxes of gravitational waves in extreme astronomical environments, and so on. Thus, high energy astrophysics makes feasible the study of the properties of matter under physical conditions which cannot yet be reproduced in the laboratory. Indeed, in many cases, the problems can only be addressed in the astrophysical environment. The aim of this book is to set out the logical sequence of steps by which astrophysicists tackle these problems.

The aim of the astrophysical sciences is two-fold – the application of the laws of physics in the extreme physical conditions encountered in astronomical systems, and the discovery of new laws of physics from observation. This second aspect has a long and distinguished pedigree, as I have recounted in my book *The Cosmic Century* (Longair, 2006). We will encounter many new and exciting examples in the course of this exposition. Throughout the text, the emphasis will be upon those aspects of high energy astrophysics in which astrophysical understanding is reasonably secure, and indicative of those areas where the astrophysics is still poorly understood.

The amount of material to be covered is enormous and so, to put some order into the presentation, the book is divided into four parts.

Part I The first part concerns the essential astronomical background needed to understand the context within which high energy astrophysical studies are carried out. If you already have a good grounding in astronomy and astrophysics, you may pass on to the subsequent parts. The first chapter introduces all the accessible astronomical wavebands and outlines the distinctive features of the astrophysical objects observed. There then follow chapters which summarise the essential features of stellar evolution, galaxies and clusters of galaxies, in order to understand the contexts within which high energy astrophysical phenomena are observed. Even studies such as the properties of galaxies have undergone a significant change of emphasis in the light of the evidence provided by very large surveys of galaxies, such as the Anglo-Australian Telescope 2dF Galaxy Survey and the Sloan Digital Sky Survey.

Part II Chapters 5–11 are principally concerned with the physical processes involved in the interactions and radiation of charged particles. The emphasis is upon a clear description of the physics of these processes. Generally, the simplest physical approach to understanding the processes is given first and then some of the more important of these are studied in more detail. Processes which dominate much of high energy astrophysics, such as bremsstrahlung, synchrotron radiation and inverse Compton scattering, merit such a more detailed treatment.

Part III Chapters 12–17 are principally concerned with high energy astrophysical processes in our Galaxy. A large suite of exotic objects is introduced, including white dwarfs, neutron stars, black holes and supernova explosions. The study of the origin of cosmic ray particles fits naturally into this discussion since these are the only samples of high energy particles originating in extreme astronomical environments which we can study directly within the Solar System. The acceleration of charged particles to high energies in Galactic environments provides clues to the much more extreme events which must take place in active galaxies.

Part IV Chapters 18–23 are devoted to extragalactic high energy astrophysics and involve some of the most extreme energetic phenomena in the Universe – the quasars, radio galaxies, TeV γ-ray sources, γ-ray bursts, and so on. The most extreme objects must involve physical processes originating close to supermassive black holes and what we observe is strongly influenced by relativistic aberration effects. In Chapter 23, some cosmological aspects of high energy astrophysics and the role that supermassive black holes may play in galaxy formation are described.

This is a very large programme and readers are encouraged to be selective in their use of the material and to customise it to their own requirements.

1.2 The sky in different astronomical wavebands

The dramatic change in perspective of astrophysical research over the last half century is conveniently illustrated by images of the celestial sphere in the different astronomical

wavebands now accessible to observation. These can be thought of as providing different temperature maps of the Universe according to Wien's displacement law,

$$\nu_{\max} = 10^{11}(T/\mathrm{K})\,\mathrm{Hz}\,; \quad \lambda_{\max} T = 3 \times 10^{6}\ \mathrm{nm\ K}\,, \tag{1.1}$$

where the relations refer to the maximum intensity of a black-body, or Planck, spectrum, expressed either in frequency or wavelength units, of a body in thermodynamic equilibrium at temperature T. These relations are shown in Fig. 1.1*a* which includes the conventional labels of the different astronomical wavebands. In the optical waveband, for example, the typical temperatures of thermal sources of radiation are about 3000–10 000 K. Thermal sources in the X-ray waveband typically have temperatures of at least 10^7–10^8 K, while far-infrared observations provide images of the cold Universe, typical temperatures being about 30–100 K. Objects with a wider range of temperatures are observable in any given waveband because of the broad-band nature of the thermal radiation spectrum. Thermodynamically speaking, the above figures are only lower limits to the temperatures of sources which are observable in these wavebands. In the case of non-thermal sources of radiation, by which we mean radiation emitted by sources which do not possess a Maxwellian energy distribution of radiating particles, the effective temperature of the emitting particles can far exceed the above temperatures. This is particularly important for non-thermal sources such as Galactic and extragalactic radio sources, quasars and X- and γ-ray sources in which the continuum radiation is associated with the emission of ultra-relativistic electrons.

Astronomical observations can be made from ground-based observatories in the optical, near-infrared, millimetre and radio wavebands. Once space was opened up for astronomical observations in the late 1950s, it became possible to observe the sky in the mid- and far-infrared, ultraviolet and X- and γ-ray wavebands. The observability of the sky in different astronomical wavebands is illustrated in Fig. 1.1*b*, which shows the transparency of the atmosphere as a function of wavelength. In this representation, the solid line indicates how high a telescope has to be located above the surface of the Earth for the atmosphere to become transparent to radiation of different wavelengths. Let us first summarise the observational challenges and the nature of the objects which dominate all-sky images in these wavebands.[1]

1.3 Optical waveband

$3 \times 10^{14} \leqslant \nu \leqslant 10^{15}$ Hz; 1 μm $\geqslant \lambda \geqslant$ 300 nm

1.3.1 Observing in the optical waveband

Until 1945, astronomy meant optical astronomy and Fig. 1.1*a* shows that this corresponds to studying the Universe in the rather narrow wavelength interval 300–800 nm, and hence to black-body temperatures in the range 3000–10 000 K. The wavelength range to which

[1] Many more details of the history of the different types of astronomy discussed in the succeeding sections of this chapter are included in my book *The Cosmic Century: A History of Astrophysics and Cosmology* (Longair, 2006).

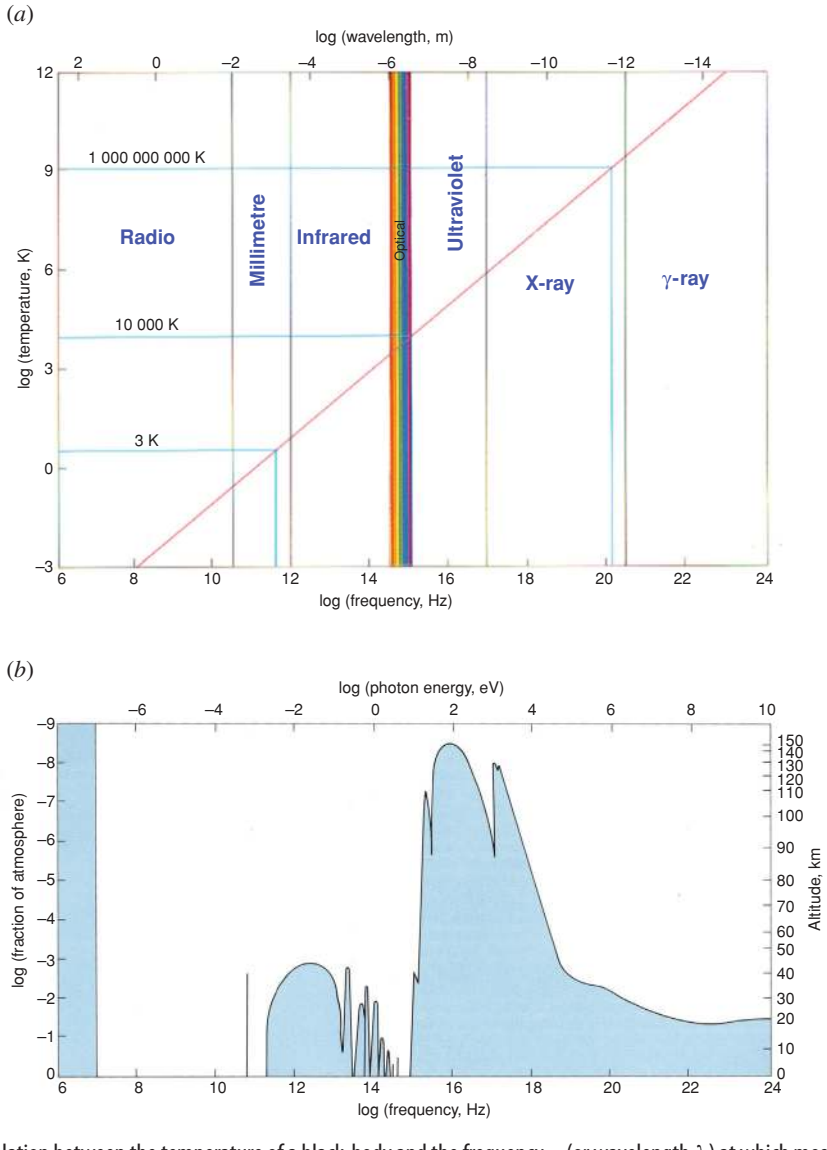

Fig. 1.1 (*a*) The relation between the temperature of a black-body and the frequency ν (or wavelength λ) at which most of the energy is emitted (solid red line). The frequency (or wavelength) plotted is that corresponding to the maximum of a black-body at temperature T. Convenient expressions for this relation are: $\nu_{\rm max} = 10^{11}(T/{\rm K})$ Hz; $\lambda_{\rm max}T = 3 \times 10^6$ nm K. The ranges of wavelength corresponding to the different wavebands – radio, millimetre, infrared, optical, ultraviolet, X- and γ-ray – are shown. (*b*) The transparency of the atmosphere for radiation of different wavelengths. The solid line shows the height above sea-level at which the atmosphere becomes transparent for radiation of different wavelengths (Giacconi *et al.*, 1968; Longair, 1988).

our eyes are sensitive is roughly 400–700 nm, corresponding to the blue and red ends of the optical spectrum, respectively. At the short wavelength end of the waveband, the atmosphere becomes opaque because of absorption by ozone in the upper atmosphere. The absorption sets in rather abruptly with decreasing wavelength so that observations from ground-based observatories at wavelengths less than about 320 nm are generally impossible. This has the beneficial effect of protecting us from the Sun's hard ultraviolet radiation. Most people derive their intuitive picture of the Universe from observations in the optical waveband.

For most types of observation, photographic plates have now been replaced by electronic detectors such as charge-coupled devices (CCD) which have quantum efficiencies of about 80% at the red end of the optical spectrum (500–1000 nm). The band-gap of silicon corresponds to a limiting maximum wavelength of about 1 μm and so optical CCDs are more or less limited to the classical optical waveband. Nowadays, it is routine to observe with CCD arrays of, say, 2000 × 2000 picture elements (pixels) and greater. Mosaics of CCD arrays can be used to provide coverage of large areas of sky, as has been achieved in the Sloan Digital Sky Survey. The result has been a huge increase in the quantity and quality of the data which can be analysed astrophysically.

When it was commissioned in the late 1940s, the Palomar 200-inch telescope was an outstanding feat of optical-mechanical engineering and it dominated much of astrophysical and cosmological research for the subsequent 30 years. Five metres was regarded as the maximum feasible aperture because the telescope had to have sufficient stiffness to track and guide accurately over the entire celestial hemisphere. By the 1980s, it was realised that the route to larger aperture was to use the increasing power of computers to build lighter telescopes and then to restore the stiffness electronically by multiply-embedded computer control systems. In so doing, much improved performance has been achieved for telescopes in the 8–10 metre class. The incorporation of *adaptive optics* into the optical train of these telescopes has meant that they can now operate close to the diffraction limit. There are now plans for even larger telescopes, the challenge being to build them at affordable cost.

1.3.2 Optical all-sky images

Images of the northern and southern celestial hemispheres are shown in Fig. 1.2*a*. These are plotted in *equidistant azimuthal polar* or *zenith equidistant projections* and were reconstructed by Mellinger from 51 wide-angle photographs (Mellinger, 2007). The image of the northern celestial hemisphere on the left has the north celestial pole at declination $\delta = 90^\circ$ in the centre, while the celestial equator, $\delta = 0^\circ$, is the bounding circle around the edge of the picture.[2] Close inspection of the image shows a number of clearly recognisable constellations, for example, the Plough or Great Bear pointing towards the North Pole star, which is close to the centre of the image. The right-hand image shows the southern celestial hemisphere, centred on the southern celestial pole at $\delta = -90^\circ$. Because two images have been used to span the whole sky, the distortions are not too great, as shown in Fig. A.3*a* of Appendix A.1. In both diagrams, the Milky Way is clearly seen as a broad band of emission spanning both hemispheres. The Galactic Centre region lies in the southern

[2] For details of the coordinate systems and projections used in astronomy, see Appendix A.1.

(*a*)

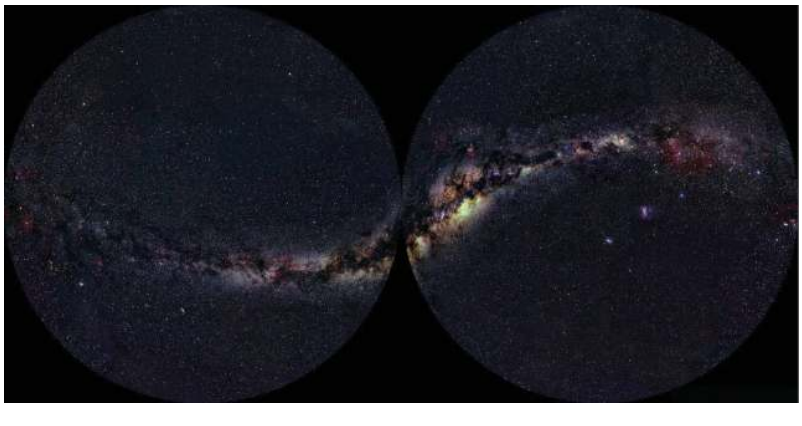

(*b*)

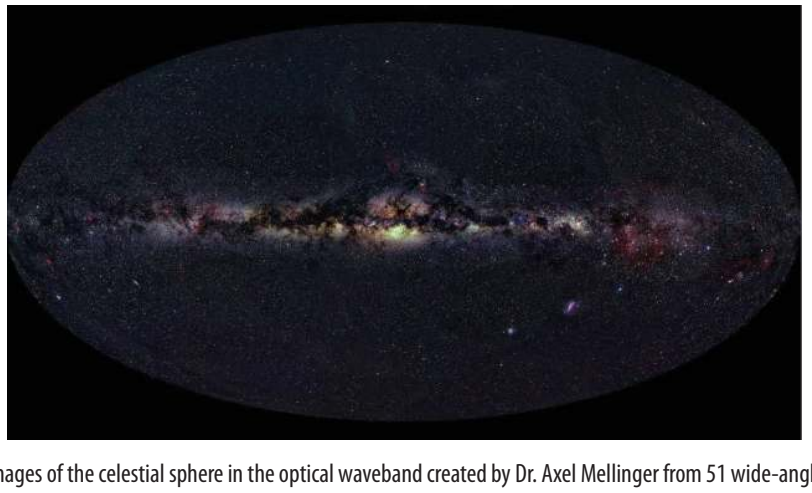

Fig. 1.2 All-sky images of the celestial sphere in the optical waveband created by Dr. Axel Mellinger from 51 wide-angle images. The photographs were taken at observing sites in California, South Africa and Germany, image processed and joined together digitally. How these images were created is explained in his web site at http://home.arcor-online.de/axel.mellinger/. (*a*) The northern (left) and southern (right) celestial hemispheres are plotted in equidistant azimuthal polar or zenith equidistant projections. The Milky Way is the broad band of emission seen in both images and is much more prominent in the southern than in the northern skies. (*b*) The optical image of the whole sky in Galactic coordinates in a Hammer–Aitoff projection. The nearby dwarf companion galaxies to our own Galaxy, the Large and Small Magellanic Clouds, are seen in the southern Galactic hemisphere at about Galactic longitudes 290° and 310°, respectively. (Courtesy of Dr. Axel Mellinger.)

celestial hemisphere at $\delta \approx -29^\circ$ and much more of the Galactic plane can be observed from that hemisphere as compared with the northern hemisphere. The two bright galaxies close to the centre of the image of the Southern Galactic Hemisphere are the Large and Small Magellanic Clouds, our nearest neighbouring galaxies.

A *Hammer–Aitoff projection* of Mellinger's observations enables the complete 4π steradians of the celestial sphere to be projected onto a two-dimensional flat surface (Fig. 1.2*b*). This projection adopts a reasonable compromise between shape and scale distortions, the

magnitude of these being indicated in Fig. A.3*b* of Appendix A.1. Although equal areas are preserved, the geometric distortions become large towards the northern and southern Galactic poles. The north and south Galactic poles ($b = \pm 90^\circ$) are at the top and bottom of the image. The scale of Galactic longitude runs from 0° at the centre, which is the direction of the Galactic Centre, through $+180^\circ$ at the left of the image, the anti-Centre direction, and then from $+180^\circ$ at the right of the image to 360° (or 0°) at the Centre. The Hammer–Aitoff projection is commonly used in the astronomical literature to display images of the whole sky, and the all-sky images in other astronomical wavebands discussed later in this chapter are presented in this projection.

The light seen in Fig. 1.2 is almost entirely the integrated light of stars. Some of the light of the Galaxy is due to hot diffuse gas, particularly the ionised gas observed in the vicinity of regions of star formation. One of the disadvantages of observing in the optical waveband is immediately apparent from Fig. 1.2. There are patchy dark features present in the image of the Milky Way and these are associated with *extinction* by interstellar dust grains. Tiny dust particles, typically about 1 μm in diameter, strongly scatter and absorb light rays, resulting in the patchy obscuration seen in Fig. 1.2*b*. Dust extinction complicates the interpretation of optical observations and corrections need to be made for it.

Optical observations are fundamental for astronomy because a significant fraction of the baryonic matter in the Universe is locked up in stars with masses within a factor of about 10 of that of the Sun and these emit a large fraction of their energy in the optical waveband. Since they have long lifetimes, they are the most readily observable objects in the Universe. The stars are assembled into galaxies and these are the basic building blocks of the Universe.

Many different types of high energy astrophysical object are present in our Galaxy, including supernovae, supernova remnants, white dwarfs, neutron stars, stellar-mass black holes and the supermassive black hole in the Galactic Centre. These are, however, often difficult to observe in the optical waveband, partly because they are intrinsically rather faint optically and also because of interstellar extinction. Optical observations are, however, crucial in identifying the sources of the radiation and understanding their roles in stellar evolution. A number of these compact stars are members of binary systems and the companion star can often be identified optically. This is of great importance in determining their distances and masses.[3]

1.4 Infrared waveband

$3 \times 10^{12} \leqslant \nu \leqslant 3 \times 10^{14}$ Hz; $100 \geqslant \lambda \geqslant 1$ μm

1.4.1 Observing in the infrared waveband

The problem of dust extinction is a strong function of wavelength, the extinction coefficient α being roughly proportional to λ^{-1}, where α is defined by $I = I_0 \mathrm{e}^{-\alpha r}$ and r is the distance

[3] More details of methods of determining distances and masses are given in Appendices A.2 and A.3.

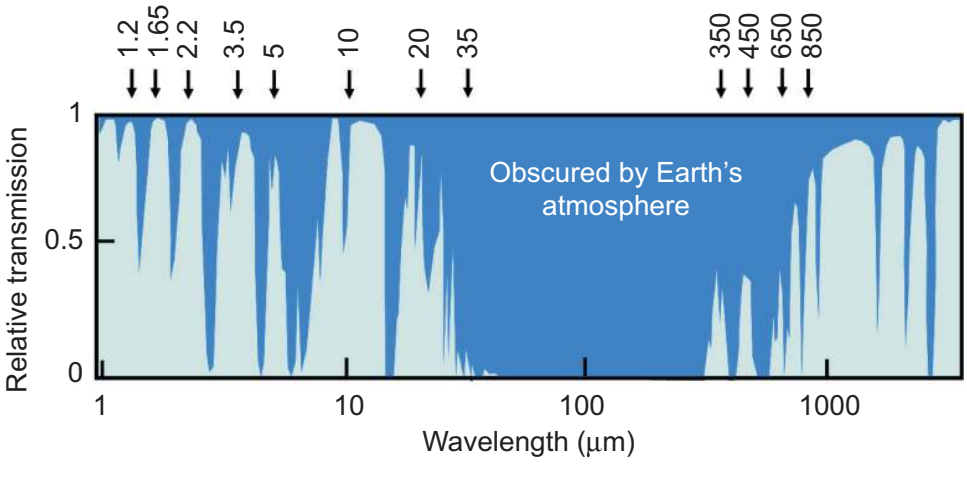

Fig. 1.3 The transmission of the atmosphere as a function of wavelength in the infrared ($1 \leqslant \lambda \leqslant 100$ μm) and submillimetre ($100 \leqslant \lambda \leqslant 1000$ μm) wavebands. The central wavelengths of the observable windows in these wavebands in microns are indicated by the numbers at the top of the diagram. The precipitable water vapour content of the atmosphere is assumed to be 1 mm. (After diagram, courtesy of the Royal Observatory, Edinburgh.)

of the source. Thus, the effects of extinction become rapidly much less important in the infrared as compared with the optical waveband. Infrared radiation suffers, however, from molecular absorption and scattering in the Earth's atmosphere, what is often referred to as *telluric absorption*, so that the sky can only be observed in certain wavelength windows. Figure 1.3 shows the transmission of the atmosphere in the waveband interval $1 \leqslant \lambda \leqslant 1000$ μm. The centres of the infrared windows in the wavelength range $1 \leqslant \lambda \leqslant 100$ μm are at wavelengths of 1.2, 1.65, 2.2, 3.5, 5, 10, 20 and 35 μm and they are conventionally labelled the J, H, K, L, M, N, Q and Z infrared wavebands, respectively. The last two windows are only accessible from very high, dry sites and even observations at 10 μm are often difficult, except under the best observing conditions. Observations outside these windows have to be undertaken from balloons, high-flying aircraft or satellite observatories. There is thus a complementarity between the types of observation attempted from the ground and from above the Earth's atmosphere.

A distinctive problem to be overcome in infrared astronomy is that the telescope and the Earth's atmosphere are strong thermal emitters of infrared radiation. For example, the radiation of a black-body at room temperature, say 300 K, peaks at a wavelength of about 10 μm. Therefore, normally, the strength of the signal from an astronomical source is very much weaker than the background due to the telescope and the atmosphere at these wavelengths. For this reason, telescopes dedicated to thermal infrared observations, such as IRAS and the Spitzer Space Telescope, incorporate cooling of the telescope and the focal plane instrumentation to minimise the thermal background.

The infrared waveband is conveniently divided into *near* and *thermal* infrared wavelengths. The distinction is related to those parts of the waveband at which the observations are detector-noise limited (the near-infrared) and those in which the thermal background

radiation from the sky and the telescope are the dominant source of noise (the thermal infrared). The distinction thus depends upon the type of observation being undertaken. Broad-band observations at wavelengths longer than 3 μm are thermal background limited, whereas those at shorter wavelengths are normally detector-noise limited. In making observations in the thermal infrared waveband, the observer is almost always searching for very faint signals against an enormous thermal background. Detector technology for infrared wavelengths has made enormous strides over the last 20 years. Infrared detector arrays almost as large as the CCD detector arrays used in optical astronomy are now available and these have revolutionised essentially all areas of astronomy.

The observing strategy is therefore to observe the sky in those wavelength windows in which there is good atmospheric transparency from ground-based telescopes. This has the advantage that the observations can be made with 8–10 metre aperture telescopes and complex instrumentation. The wavebands which are inaccessible from the ground have to be observed from above the Earth's atmosphere, preferably from satellite observatories. Necessarily, these are generally smaller than the ground-based telescopes and massive instrumentation cannot be accommodated. The Spitzer Infrared Space Telescope is a splendid example of the state-of-the-art in infrared space technology. In due course it will be superseded by the James Webb Space Telescope, which will be a 6.5 metre infrared-optimised space telescope.

1.4.2 Infrared all-sky images

Images of the whole sky in the near-infrared waveband have much reduced interstellar extinction by interstellar dust grains and the structure of our Galaxy can be clearly seen. Figures. 1.4*a* and *b* provide excellent examples of the structure of the Galaxy as observed in the 1.2–2.2 μm wavebands. Figure 1.4*a* is an all-sky image obtained by the DIRBE instrument of the Cosmic Background Explorer (COBE). This instrument scanned the sky in the J, H and K wavebands and these were combined to create the colour image seen in Fig. 1.4*a*. The disc and bulge of the Galaxy are clearly seen, as well as a thin dust absorption layer lying in the Galactic plane.

Figure 1.4*b* shows another approach to mapping the Galaxy using observations from the ground-based Two Micron All-Sky Survey (2MASS). This survey was carried out using two 1.3 metre dedicated infrared telescopes, one located at Mount Hopkins in Arizona and the other at the Cerro Tololo InterAmerican Observatory in Chile. Almost 300 million stars were catalogued. The image shown in Fig. 1.4*b* was created by plotting the positions of almost 100 million stars brighter than $K = 13.5$ from the 2MASS catalogue. This approach provides an even clearer image of the stellar distribution in the Galaxy. The Large and Small Magellanic Clouds are clearly visible in the southern Galactic hemisphere, as is the elongated central bulge of the Galaxy which has been interpreted as a bar in the central regions of the Galaxy. These images make the important point that, in the infrared waveband, interstellar dust becomes transparent and so it is possible to observe deep inside regions which are obscured at optical wavelengths. Among the most important of these are regions of star formation which are enshrouded in interstellar dust, and the very central regions of our own Galaxy. Observations of infrared stars very close to the Galactic Centre have provided wholly convincing evidence for a supermassive black hole with mass $M \approx 2.6 \times 10^6\ M_\odot$.